Theoretical and Computational Analysis of Airflow-Induced Leaf Collection Mechanism in a Selective Tea Harvesting End-Effector

Sharamjeet Shaurya[1], Arjun Agarwal[2], Dhirendra Kumar Verma[3], Kamal Narayan Baruah[4], Jyotindra Narayan[5]

***Abstract*— Traditional tea harvesting methods often lack precision, leading to significant leaf damage and reduced operational efficiency. To address these limitations, this paper proposes an airflow-driven end-effector designed for selective tea harvesting, utilizing pneumatic transport to move harvested leaves from the shearing interface to storage. A theoretical model based on force equilibrium was developed to determine the critical transport velocity (CTV), calculated to be approximately 3.6 m/s. The theoretical prediction was further evaluated through CFD analysis using ANSYS Fluent with a k–ω Shear Stress Transport (SST) turbulence model across inlet velocities ranging from 2.5 m/s to 4.5 m/s. Simulation results indicate that inlet velocities at or above 3.6 m/s provide airflow conditions favourable for sustained pneumatic leaf transport, with 4.5 m/s achieving outlet velocities up to 6.586 m/s and mass flow rates of approximately 1.59×10^{-3} kg/s, while lower velocities fail to maintain sufficient transport momentum. Despite considerable velocity decay along the transport path, adequate velocity is retained in critical regions for sustained pneumatic conveyance. These findings demonstrate the feasibility of airflow-based transport for selective harvesting and provide a quantitative basis for optimizing end-effector design.**

I. INTRODUCTION

Camellia Sinensis, often referred to as tea, is one of the most widely consumed beverages in the world and holds a significant place in various cultures. Tea is nutrient-rich and contains high levels of antioxidants that help fight free radicals, promoting cellular health. The annual global tea production, measured in fresh harvest weight, is approximately 32 million tons (mT). As reported by the Food and Agriculture Organization (FAO) in 2024, China remains the largest tea producer globally, with an annual production of 14.5 mT, followed by India, producing approximately 5.97 mT annually, while Kenya, Sri Lanka, and Türkiye contributed 2.33 mT, 1.40 mT, and 1.30 mT, respectively. However, the tea industry faces a challenge in balancing maximizing harvest yield with maintaining high quality. At present, tea harvesting is labour-intensive and involves tedious, repetitive actions. Workers manually collect tea leaves from different zones every 6–7 days, making it a costly operation that accounts for nearly 35% of total production costs worldwide [1]. For optimal tea quality, it is crucial to precisely identify the plucking points of tea shoots. High-quality tea production typically involves harvesting two or three leaves with a bud; however, a bud with two leaves is generally regarded as superior in quality compared with a bud with three leaves. Furthermore, the internodal region of the tea shoot, as shown in Fig. 1, is considered a major natural dietary source of L-theanine, a distinctive non-protein amino acid that acts as an antidepressant and improves sleep cycle [2]. Achieving this plucking standard relies on laborers' skill levels, which can be inefficient and error-prone. The literature identifies two main categories of mechanical harvesters, hand-held and ride-on, for tea plucking as an alternative to overcome the labor shortages. The evolution of tea harvesting machinery has brought about several benefits, including increased efficiency, greater productivity, reduced labor requirements, and scalability [3].

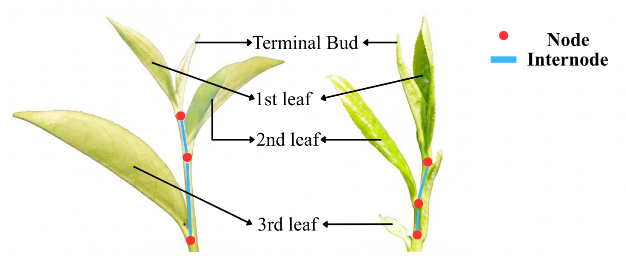

Fig. 1. Morphological structure of a tea shoot showing the terminal bud, leaves, nodes, internodes, and the targeted selective harvesting region used for airflow-assisted collection.

Recent research in mechanised tea harvesting has explored an advanced canopy-following cutting technique to improve cutting consistency. Incremental Proportional–Integral–Derivative (PID) control has been applied in self-actuated tea harvesters to continuously regulate cutter height and header tilt for uniform canopy trimming [4]. A Delta parallel manipulator-based automated tea plucking system has been proposed, wherein the manipulator plays a central role in executing precise trajectory tracking and harvesting operations, demonstrating effective performance but with limitations in positioning accuracy and operational efficiency [5]. To further enhance harvesting performance, an under-actuated end-effector was optimised by analysing the physical and mechanical properties of tea buds and

[1,2,3]Sharamjeet Shaurya, Arjun Agarwal, Dhirendra Kumar Verma are with Department of Computer Science and Mechanical Engineering, Sharda University, Greater Noida, Uttar Pradesh, India [1]ryugandhar.of@outlook.com, [2]arjun.agra76@gmail.com, [3]vermadk.iitg@gmail.com

[4]Kamal Narayan Baruah is with Tea Processing and Manufacturing Advisory Department, Tocklai Tea Research Institute TRA, 785008, Jorhat, Assam, India [4]kamalnarayan@tocklai.net

[5]Jyotindra Narayan is with the Smart & Healthcare Laboratory, Department of Mechanical Engineering, IIT Patna, Patna, Bihar, India [5]jnarayan@iitp.ac.in

refining the structural design through geometric constraints and optimisation techniques [6]. To address terrain variability, a tea canopy surface profiling method based on 2D LiDAR perception has been proposed, enabling accurate canopy reconstruction and adaptive cutter height control. Field experiments demonstrated improved harvesting performance and higher bud-leaf integrity compared to conventional systems [7]. Despite these advancements, most existing tea harvesting machines rely on top-layer shearing using blades, resulting in non-selective harvesting suited for bulk production rather than high-quality selective plucking [8]. Although improvements in operational stability have been reported, current approaches remain largely dependent on ground-based systems, leaving the aforementioned challenges inadequately addressed, which could potentially be overcome through aerial deployment of the end effector [9]. Additionally, mechanical harvesters can damage tea leaves by shearing them not through the shoots but through the leaf itself, leading to an oxidation of the tea leaf and a reduction in tea leaf quality. To enable selective harvesting under irregular terrain conditions, this work considers a Unmanned Aerial Vehicle (UAV) assisted robotic harvesting system in which the UAV provides aerial mobility while the attached end-effector performs selective cutting and pneumatic leaf transport. Such aerial deployment improves accessibility and operational flexibility in tea plantations [10].

Based on the aforementioned limitations, this work presents the novel design and Computational fluid dynamics (CFD) assisted analysis of an airflow-driven end-effector for selective tea harvesting with pneumatic leaf transport, aimed at reducing leaf damage and improving picking efficiency. A key contribution is the identification of the critical transport velocity of about 3.6 m/s, which serves as a quantitative threshold for effective leaf conveyance. Through CFD-based evaluation over multiple inlet velocities, the study shows that airflow rates of 3.6–4.5 m/s provide sufficient mass flow and momentum for effective pneumatic conveyance. Overall, the work establishes the feasibility of air-based selective harvesting and offers a design basis for optimizing pneumatic tea-harvesting end-effectors. The rest of this paper is organized as follows: Section 2 presents the design and working mechanism, Section 3 covers the CFD and theoretical analysis, Section 4 discusses the results, and Section 5 concludes the study.

II. System Design and Considerations

The proposed system is a drone-assisted selective tea harvesting platform integrating a multi-rotor UAV with a rectangular harvesting module. The module combines a BLDC-driven reciprocating cutting mechanism and a pneumatic transport system to collect severed leaves into an onboard storage chamber. Shoot detection is performed using a YOLOv8-based deep learning model [11].

A. System Architecture

The system integrates a multirotor UAV, a reciprocating cutting mechanism, a pneumatic transport chamber, and a vision-based detection system, as shown in Fig. 2. The UAV follows predefined waypoints, detects harvestable shoots, performs selective cutting, and returns to dock when storage or battery limits are reached.

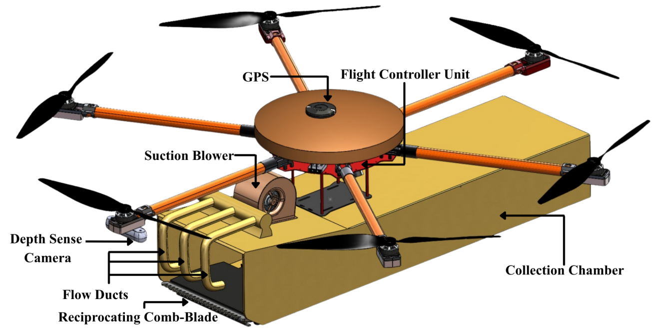

Fig. 2. UAV-based selective tea harvesting end-effector showing the integrated cutting mechanism, airflow guiding ducts, centrifugal blower, and collection chamber for efficient leaf transport.

B. UAV Platform, Mounting, Fabrication, and Materials

A multirotor UAV platform is selected for its payload capacity and stability [12]. The harvesting module is mounted beneath the airframe using a vibration-damped PLA/ABS bracket fabricated via FDM, while the cutting components are manufactured using Wire-EDM for precision and durability [13]. The overall design is optimized to achieve a balance between lightweight construction and durability for efficient field deployment.

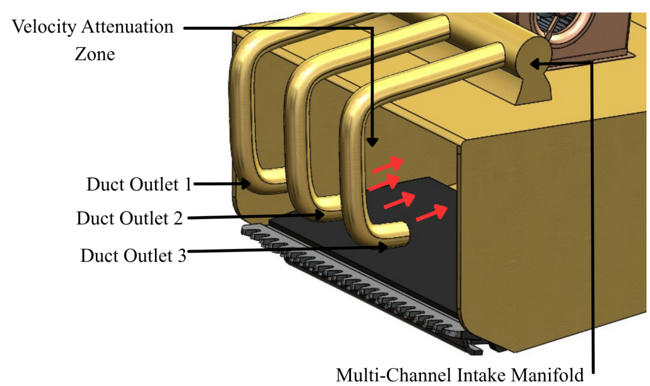

Fig. 3. Detailed view of the multi-channel intake manifold showing duct outlets and airflow direction into the transport chamber, highlighting the velocity attenuation zone.

C. Harvesting Module and Cutting Mechanism

The module is a rectangular enclosure designed to guide airflow efficiently toward the storage chamber as shown in Fig. 3. A reciprocating comb-blade mechanism, driven by a BLDC motor and eccentric linkage, performs shoot severance. This mechanism enables uniform cutting across the aperture without requiring precise UAV alignment. The clean shearing action minimizes leaf damage and preserves quality [14].

D. Pneumatic Transport, Storage, and Docking Mechanism

A front-mounted pneumatic hose generates an inward air jet using a centrifugal blower, where the airflow entrains severed shoots and transports them through the internal channel into the storage chamber. The geometry is designed to efficiently direct airflow from the cutting zone to the storage region, supporting sustained pneumatic conveyance. The upper chamber stores harvested leaves and incorporates a mesh outlet to allow airflow exit, while a proximity sensor monitors the fill level and triggers return-to-dock operation when required. At the docking station, leaves are discharged pneumatically, after which the UAV resumes harvesting operations.

E. Vision-Based Detection and Control

A YOLOv8-based vision system is used to identify harvestable shoots under varying field conditions [15]. Detected targets guide UAV positioning, while an incremental PID controller maintains stable flight during harvesting operations [16], [17].

III. Methodology

A. Theoretical Modeling of Airflow-Induced Transport

The pneumatic transport mechanism relies on airflow momentum to overcome gravitational and resistive forces acting on harvested tea leaves and to transport them from the cutting region to the collection chamber. To determine the minimum airflow required for sustained pneumatic conveyance, a theoretical force-equilibrium model was developed to estimate the critical transport velocity (CTV).

The objective is to determine the minimum velocity required for reliable lift-off and transport of tea leaves:

$$U_{in} \geq U_{crit} \tag{1}$$

where U_{crit} represents the threshold velocity required to initiate motion.

A tea leaf begins to move when the aerodynamic drag force overcomes its weight. The governing condition is:

$$F_D \geq F_g \tag{2}$$

The drag force acting on the leaf is given by:

$$F_D = \frac{1}{2} C_D \rho A_{eff} U^2 \tag{3}$$

where C_D is the drag coefficient, ρ is the air density, A_{eff} is the effective projected area, and U is the inlet velocity.

The gravitational force is expressed as:

$$F_g = mg \tag{4}$$

1) Leaf Area Model: To represent the geometry of tea leaves, each leaf is approximated as an ellipse. The area of a single leaf is given by:

$$A_i = \frac{\pi}{4} L_i W_i \tag{5}$$

where $W_i = kL_i$ represents the leaf width, assumed proportional to its length, and A_i denotes the projected leaf area. Substituting, the area becomes:

$$A_i = \frac{\pi}{4} k L_i^2 \tag{6}$$

Since leaves are inclined relative to the airflow, the effective projected area is reduced. This is accounted for using:

$$A_{eff,i} = A_i \cos(\beta_i) \tag{7}$$

For a multi-leaf system, the total effective area is:

$$A_{eff} = \frac{\pi}{4} k \sum_{i=1}^{3} L_i^2 \cos(\beta_i) \tag{8}$$

For simplification, the first and second leaves are assumed to exhibit similar inclination characteristics and are therefore represented using the same inclination angle β_1, while the third leaf is represented by β_2. The one-bud-three-leaf case is treated as the worst case because it gives the largest exposed area and, therefore, the highest drag during transport. Here, L_1 is the base-to-first-leaf length, L_2 is the spacing to the second leaf, L_3 is the length up to the third leaf, L_4 is the internode spacing, and β_1, β_2 denote the leaf-blade inclination angles.

To obtain representative geometric parameters for the analysis, data for these quantities were extracted from [18]. The reported measurements across multiple tea cultivars were used to compute mean values, expressed as:

$$\bar{L}_i = \frac{1}{n} \sum_{j=1}^{n} L_{i,j} \tag{9}$$

$$\bar{\beta}_i = \frac{1}{n} \sum_{j=1}^{n} \beta_{i,j} \tag{10}$$

where n is the number of samples, and $L_{i,j}$ and $\beta_{i,j}$ denote the measured length and inclination angle for the j-th sample.

2) Critical Transport Velocity: Substituting the effective area into the force balance:

$$\frac{1}{2} C_D \rho A_{eff} U_{crit}^2 = mg \tag{11}$$

Rearranging:

$$U_{crit} = \sqrt{\frac{2mg}{C_D \rho A_{eff}}} \tag{12}$$

B. CFD Methodology

To evaluate airflow behaviour within the proposed end-effector, a three-dimensional computational fluid dynamics (CFD) analysis was performed using ANSYS Fluent. The aim of the simulation was to study velocity distribution, flow structure, and internal airflow characteristics under varying inlet conditions. The airflow was modelled as incompressible, and turbulence effects were captured using the k–ω (Shear Stress Transport) (SST) turbulence model. The turbulence model was selected due to its suitability for internal duct flows involving adverse pressure gradients, curvature, and localized flow separation, which are expected within the ducted geometry of the end-effector.

A steady-state approach was adopted, and each simulation case was run for 500 iterations. Convergence was ensured by monitoring the reduction of residuals for the governing equations and by verifying the stabilisation of key output parameters such as outlet velocity and mass flow rate. The computational domain includes the airflow ducts, suction blower region, and collection chamber. The computational domain was discretised using an unstructured tetrahedral mesh consisting of approximately 1.0×10^5 elements, which provided stable convergence behaviour and consistent outlet flow characteristics during preliminary mesh refinement evaluation. Velocity inlet boundary conditions were imposed at the inlet for airflow velocities ranging from 2.5 m/s to 4.5 m/s, while pressure outlet conditions were specified at the outlet planes. No-slip wall conditions were applied along the internal duct surfaces. The velocity decay within the system was evaluated to assess airflow's effectiveness in transporting tea leaves from the cutting region to the collection chamber. The decay was quantified using:

$$\text{Velocity Decay (\%)} = \frac{V_{\text{inlet}} - V_{\text{plane}}}{V_{\text{inlet}}} \times 100 \qquad (13)$$

This CFD framework provides the basis for analysing airflow characteristics and assessing whether the system meets the critical transport velocity requirement for effective tea leaf collection.

IV. Results and Discussion

A. Theoretical Analysis Results

The theoretical model developed in the methodology section was used to estimate the critical transport velocity (CTV) required for effective leaf motion. Substituting the representative geometric and physical parameters into the derived expression:

$$U_{crit} = \sqrt{\frac{2 \cdot 0.00353 \cdot 9.81}{1.1 \cdot 1.225 \cdot 0.00383}} \qquad (14)$$

$$U_{crit} = 3.6 \text{ m/s} \qquad (15)$$

This value represents the minimum airflow velocity required to initiate leaf motion under worst-case conditions. The theoretical CTV serves as a reference for evaluating CFD simulation results and determining the operational threshold for reliable leaf transport.

The mean geometric parameters obtained from the Eqs. (9)-(10) are: $\bar{L}_1 = 0.0687\,\text{m}$, $\bar{L}_2 = 0.0292\,\text{m}$, $\bar{L}_3 = 0.0917\,\text{m}$, and $\bar{L}_4 = 0.0324\,\text{m}$, with corresponding inclination angles $\bar{\beta}_1 = 28.58°$ and $\bar{\beta}_2 = 29.70°$. From these values, the derived trigonometric parameters are: $\cos\bar{\beta}_1 = 0.878$ and $\cos\bar{\beta}_2 = 0.869$. The physical parameters used in the analysis include: $k = 0.4$, leaf mass $m = 0.00353\,\text{kg}$, air density $\rho = 1.225\,\text{kg/m}^3$ taken from [19], drag coefficient $C_D = 1.1$, and gravitational acceleration $g = 9.81\,\text{m/s}^2$.

The results obtained from the CFD simulations are presented and analysed to evaluate the airflow behaviour within the tea harvesting end-effector and its effectiveness in transporting tea leaves from the cutting region to the collection chamber.

B. CFD Results

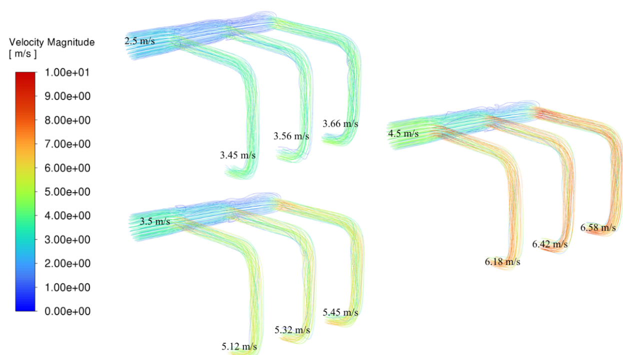

Fig. 4. Pathline visualisation of airflow at inlet velocities of 2.5 m/s, 3.5 m/s, and 4.5 m/s, representing conditions below, near, and above the critical transport velocity (3.6 m/s).

Fig. 4 presents airflow pathline visualisations for inlet velocities of 2.5 m/s, 3.5 m/s, and 4.5 m/s. Lower inlet velocities exhibit weaker flow continuity and reduced penetration through the transport pathway, while higher inlet velocities produce more coherent airflow patterns and improved flow development towards the outlet region. These results indicate improved transport conditions at higher inlet velocities. A similar analysis of the internal flow field is presented in Fig. 5, showing pathline visualisations within the collection chamber for three representative inlet conditions corresponding to 3.5 m/s, 3.0 m/s, and 4.5 m/s cases. The flow entering the chamber exhibits a change in direction and expansion, resulting in the formation of recirculation regions within the enclosure. For the lower velocity case, the flow remains relatively weak, with limited penetration into the chamber and more pronounced recirculation zones. As the inlet velocity increases, the flow exhibits stronger momentum and improved penetration towards the outlet, with more defined streamlines and reduced dispersion. The presence of recirculation within the chamber indicates energy dissipation and redistribution of airflow before exiting through the outlet. These variations highlight the influence of inlet velocity on

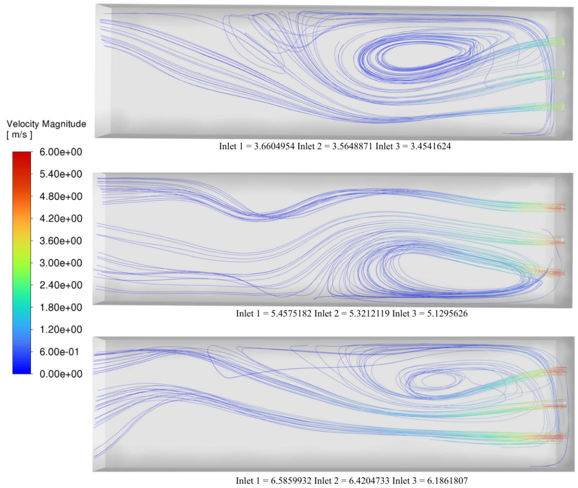

Fig. 5. Comparison of airflow pathlines inside the collection chamber for inlet velocities of 2.5 m/s, 3.5 m/s, and 4.5 m/s.

internal flow structure and transport characteristics within the collection chamber.

TABLE I

OUTLET VELOCITY AND MASS FLOW RATE FOR DIFFERENT INLET CONDITIONS

Inlet Velocity (m/s)	Outlet	Velocity (m/s)	Mass Flow Rate (kg/s)
2.5	1	3.660	8.833×10^{-4}
2.5	2	3.564	8.601×10^{-4}
2.5	3	3.454	8.330×10^{-4}
3.0	1	4.395	1.061×10^{-3}
3.0	2	4.274	1.032×10^{-3}
3.0	3	4.136	9.984×10^{-4}
3.5	1	5.129	1.239×10^{-3}
3.5	2	4.986	1.204×10^{-3}
3.5	3	4.820	1.164×10^{-3}
4.0	1	5.855	1.415×10^{-3}
4.0	2	5.705	1.377×10^{-3}
4.0	3	5.504	1.330×10^{-3}
4.5	1	6.586	1.592×10^{-3}
4.5	2	6.420	1.550×10^{-3}
4.5	3	6.186	1.495×10^{-3}

Table I presents the outlet velocity and mass flow rate for different inlet conditions. It can be observed that as the inlet velocity increases, the outlet velocity and mass flow rate also increase proportionally. The consistency across the three outlets indicates uniform flow distribution within the end-effector channels, which is essential for balanced leaf transport. Table II presents the variation of localized airflow velocity within the transport chamber for different inlet velocity conditions. These values correspond to averaged velocities at selected chamber planes and should not be interpreted as the inlet entrainment velocity predicted by the analytical model. A consistent decay in velocity is observed from the inlet region (y = 0.0) to the outlet due to viscous effects, flow separation, and internal recirculation. However, higher inlet velocities result in increased velocity levels throughout the domain, ensuring sufficient momentum for leaf transport. The results indicate that inlet velocities below the critical transport velocity lead to significantly reduced velocities near the outlet, while inlet velocities at or above the critical value maintain sufficient flow strength for sustained pneumatic conveyance.

TABLE II

VELOCITY DECAY AND MASS FLOW RATE ALONG THE TRANSPORT PATH FOR DIFFERENT INLET VELOCITY CASES

Inlet Case	**Plane (y)**	**Velocity (m/s)**	**Mass Flow (kg/s)**
2.5 m/s	0.0	0.504	0.00542
2.5 m/s	0.4	0.321	0.00553
2.5 m/s	0.8	0.114	0.00547
2.5 m/s	Outlet	0.092	0.00537
3.0 m/s	0.0	0.590	0.00650
3.0 m/s	0.4	0.330	0.00638
3.0 m/s	0.8	0.158	0.00650
3.0 m/s	Outlet	0.127	0.00639
3.5 m/s	0.0	0.659	0.00833
3.5 m/s	0.4	0.438	0.00846
3.5 m/s	0.8	0.137	0.00782
3.5 m/s	Outlet	0.131	0.00798
4.0 m/s	0.0	0.693	0.00870
4.0 m/s	0.4	0.316	0.00916
4.0 m/s	0.8	0.140	0.00849
4.0 m/s	Outlet	0.139	0.00864
4.5 m/s	0.0	0.847	0.00968
4.5 m/s	0.4	0.577	0.00921
4.5 m/s	0.8	0.214	0.00969
4.5 m/s	Outlet	0.175	0.00959

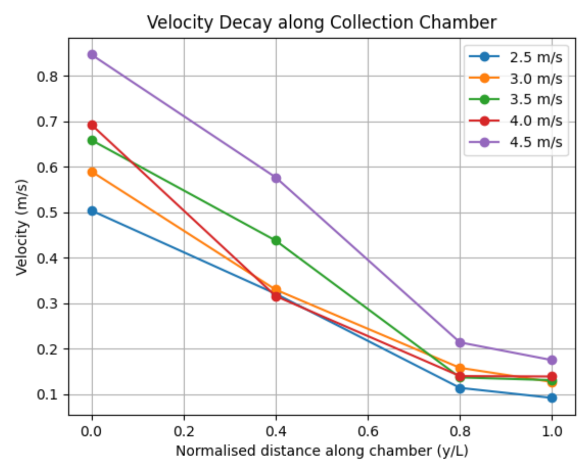

Fig. 6. Variation of airflow velocity along the collection chamber with respect to normalised distance for different inlet conditions.

For the near-critical inlet velocity case (3.5 m/s), a significant reduction in velocity is observed along the flow path. The velocity decreases from 0.659 m/s at $y = 0.0$ to 0.438 m/s at $y = 0.4$, and further to 0.137 m/s at $y = 0.8$, finally reaching 0.131 m/s at the outlet. This corresponds to an overall velocity decay of approximately 81–96%. Despite this substantial decay, the airflow in the initial and intermediate regions remains sufficiently strong to initiate and sustain leaf motion. The regions near $y = 0.0$ and $y = 0.4$ play a critical role in providing the required momentum transfer, where the leaves are entrained and guided into the transport pathway. As illustrated in Fig. 6, the airflow velocity decreases progressively along the chamber, with the most significant reduction occurring beyond the intermediate region. At inlet velocities below the critical value (2.5 m/s), the available momentum is insufficient, resulting in lower velocities across all planes and reduced capability to transport leaves effectively. This is reflected in the lower velocity magnitudes and weaker flow structures observed in the corresponding simulations. For inlet conditions near the critical velocity (3.5 m/s), the airflow maintains adequate momentum through the inlet and intermediate regions, ensuring that airflow conditions remain favourable for sustained pneumatic conveyance towards the collection chamber. The relatively higher velocity levels in the initial portion of the chamber support this observation and support the theoretical estimation of the critical transport velocity. At higher inlet velocities (4.0–4.5 m/s), an increase in absolute velocity is observed across all planes. However, the relative decay trend remains similar, indicating that the system inherently dissipates energy due to geometric complexity and flow turning. While higher velocities improve flow intensity, they do not proportionally enhance transport efficiency, suggesting diminishing returns beyond the critical velocity.

Overall, the decay analysis highlights that sustained pneumatic conveyance is governed not by maintaining high velocity throughout the domain, but by ensuring sufficient momentum in the early stages of flow to initiate and sustain leaf movement through the system. The confined duct geometry further contributes to sustained conveyance by restricting lateral dispersion and preserving directional airflow momentum within the transport pathway despite substantial downstream velocity attenuation.

V. Conclusion

This study demonstrates the theoretical and aerodynamic feasibility of an airflow-driven end-effector for selective tea harvesting. A critical transport velocity of approximately 3.6 m/s was established through theoretical modelling, providing a quantitative reference for pneumatic leaf entrainment. CFD simulations performed over inlet velocities ranging from 2.5 m/s to 4.5 m/s indicate that sufficient airflow momentum can be maintained within critical regions of the transport pathway to support sustained pneumatic conveyance despite substantial downstream velocity decay. The application of the k–ω SST turbulence model further highlights the impact of internal geometry on flow stability and energy efficiency, while the overall results provide a systematic framework for optimizing mechanical harvesting parameters to reduce leaf damage and labor costs. The present work evaluates airflow behaviour within the harvesting chamber using a simplified analytical model and single-phase CFD analysis. Coupled particle-fluid interactions, leaf collisions, deformation effects, and experimental field validation were not considered in the current study and remain important areas for future investigation. Future work will focus on prototype development and experimental validation of the proposed harvesting system under realistic tea harvesting conditions.

References

[1] L. Yan, K. Wu, J. Lin, X. Xu, J. Zhang, X. Zhao, J. Tayor, and D. Chen, "Identification and picking point positioning of tender tea shoots based on mr3p-ts model," *Frontiers in Plant Science*, vol. 13, p. 962391, 2022.

[2] L. Paiva, E. Lima, M. Motta, M. Marcone, and J. Baptista, "Variability of antioxidant properties, catechins, caffeine, l-theanine and other amino acids in different plant parts of azorean camellia sinensis," *Current Research in Food Science*, vol. 3, pp. 227–234, 2020.

[3] S. B. Salvatian, F. Soheili-Fard, and K. M. Salimi, "Effect of mechanical plucking height on tea green leaf yield and its quality." 2014.

[4] D. Zhang, R. Zhang, L. Chen, L. Zhang, T. Yi, and Q. Feng, "Adaptive tracking and cutting control system for tea canopy: Design and experimental evaluation," *Agriculture*, vol. 15, no. 5, p. 557, 2025.

[5] H. Yang, L. Chen, Z. Ma, M. Chen, Y. Zhong, F. Deng, and M. Li, "Computer vision-based high-quality tea automatic plucking robot using delta parallel manipulator," *Computers and Electronics in Agriculture*, vol. 181, p. 105946, 2021.

[6] L. Guichao, Z. Xiaoxin, Z. Wenyong, H. Zijian, L. Wangheng, and Z. Lixue, "Optimization design and testing of under-actuated tea harvesting end-effector," *Nongye Jixie Xuebao/Transactions of the Chinese Society of Agricultural Machinery*, vol. 56, no. 1, 2025.

[7] Y. Li, S. Wu, L. He, J. Tong, R. Zhao, J. Jia, J. Chen, and C. Wu, "Development and field evaluation of a robotic harvesting system for plucking high-quality tea," *Computers and Electronics in Agriculture*, vol. 206, p. 107659, 2023.

[8] S. Firouzi and F. Azarian, "Propellants of mechanical pruning and plucking of tea (a case of developing countries)," *Information Processing in Agriculture*, vol. 6, no. 4, pp. 454–461, 2019.

[9] Z. Du, D. Li, J. Ji, L. Zhang, X. Li, and H. Wang, "Bionic optimization design and experiment of reciprocating cutting system on single-row tea harvester," *Agronomy*, vol. 12, no. 6, p. 1309, 2022.

[10] S.-M. Wang, C.-P. Yu, J.-H. Ma, J.-X. Ouyang, Z.-M. Zhao, Y.-M. Xuan, D.-M. Fan, J.-F. Yu, X.-C. Wang, and X.-Q. Zheng, "Tea yield estimation using uav images and deep learning," *Industrial Crops and Products*, vol. 212, p. 118358, 2024.

[11] S. Xie and H. Sun, "Tea-yolov8s: A tea bud detection model based on deep learning and computer vision," *Sensors*, vol. 23, no. 14, p. 6576, 2023.

[12] T. L. Mien, T. N. Tu, and V. Van An, "Cascade pid control for altitude and angular position stabilization of 6-dof uav quadcopter." *International Journal of Robotics & Control Systems*, vol. 4, no. 2, 2024.

[13] W. Zhang, Y. Chen, Q. Wang, and J. Chen, "Researches on the tender leaf identification and mechanically perceptible plucking finger for high-quality green tea," *Journal of the Science of Food and Agriculture*, vol. 105, no. 4, pp. 2169–2178, 2025.

[14] S. Piyathissa, P. Kahandage, P. Dissanayake, and M. Rambanda, "Selective tea plucking machine to reduce the labor involvement," 2015.

[15] X. Tang, L. Tang, J. Li, and X. Guo, "Enhancing multilevel tea leaf recognition based on improved yolov8n," *Frontiers in Plant Science*, vol. 16, p. 1540670, 2025.

[16] I. Lebedev, A. Erashov, and A. Shabanova, "Accurate autonomous uav landing using vision-based detection of aruco-marker," in *International Conference on Interactive Collaborative Robotics*. Springer, 2020, pp. 179–188.

[17] A. Noordin, M. A. Mohd Basri, and Z. Mohamed, "Real-time implementation of an adaptive pid controller for the quadrotor mav embedded flight control system," *Aerospace*, vol. 10, no. 1, p. 59, 2023.

[18] Y. Luo, Q. Yu, Y. Xie, C. Xu, L. Cheng, Q. Shi, Y. Li, X. Zhang, and Z. Shen, "Internode length is correlated with ga3 content and is crucial to the harvesting performance of tea-picking machines," *Plants*, vol. 12, no. 13, p. 2508, 2023.

[19] H. Chen, C.-J. Liu, C.-F. Liu, C.-Y. Hu, M.-C. Hsiao, M.-T. Chiou, Y.-S. Su, and H.-T. Tsai, "A growth model to estimate shoot weights and leaf numbers in tea," *Agronomy Journal*, vol. 111, no. 5, pp. 2255–2262, 2019.